



## OPEN ACCESS

## EDITED BY

Tomaso Fortibuoni,  
Istituto Superiore per la Protezione e  
la Ricerca Ambientale (ISPRA), Italy

## REVIEWED BY

Dimitris Velaoras,  
Hellenic Centre for Marine Research  
(HCMR), Greece  
Milena Menna,  
Istituto Nazionale di Oceanografia e di  
Geofisica Sperimentale, Italy  
Maurizio AZZARO di Rosamarina,  
National Research Council (CNR), Italy

## \*CORRESPONDENCE

T. Ozer  
tal@ocean.org.il  
B. Herut  
barak@ocean.org.il

## SPECIALTY SECTION

This article was submitted to  
Marine Fisheries, Aquaculture and  
Living Resources,  
a section of the journal  
Frontiers in Marine Science

RECEIVED 01 June 2022

ACCEPTED 29 June 2022

PUBLISHED 27 July 2022

## CITATION

Ozer T, Rahav E, Gertman I, Sisma-  
Ventura G, Silverman J and Herut B  
(2022) Relationship between  
thermohaline and biochemical  
patterns in the levantine upper and  
intermediate water masses,  
Southeastern Mediterranean Sea  
(2013–2021).  
*Front. Mar. Sci.* 9:958924.  
doi: 10.3389/fmars.2022.958924

## COPYRIGHT

© 2022 Ozer, Rahav, Gertman, Sisma-  
Ventura, Silverman and Herut. This is an  
open-access article distributed under  
the terms of the [Creative Commons  
Attribution License \(CC BY\)](https://creativecommons.org/licenses/by/4.0/). The use,  
distribution or reproduction in other  
forums is permitted, provided the  
original author(s) and the copyright  
owner(s) are credited and that the  
original publication in this journal is  
cited, in accordance with accepted  
academic practice. No use,  
distribution or reproduction is  
permitted which does not comply with  
these terms.

# Relationship between thermohaline and biochemical patterns in the levantine upper and intermediate water masses, Southeastern Mediterranean Sea (2013–2021)

T. Ozer\*, E. Rahav, I. Gertman, G. Sisma-Ventura,  
J. Silverman and B. Herut\*

Israel Oceanographic and Limnological Research, National Institute of Oceanography, Haifa, Israel

The relationships between the interannual variations of the Levantine intermediate water (LIW) core properties and the corresponding biochemical variations in the euphotic zone were systematically studied in the Southeastern Mediterranean during 2013–2021 and since 2002 based on a previous study. Salinity and temperature interannual fluctuations in the LIW continue to follow the Adriatic–Ionian Bimodal Oscillating System (BiOS) mechanism, with salinity and temperature peaks in the years 2008–2010, 2014–2015, and 2018–2019 coinciding with periods of anticyclonic circulation of the North Ionian Gyre (NIG). During these anticyclonic periods, the transport of Atlantic Water into the Levant is reduced together with the transport of LIW out of the basin. These interannual fluctuations are superimposed on a long-term warming trend clearly evident from previous studies, showing a maximal temperature in 2018–2019, higher than the previously mentioned temperature peaks by  $\sim 0.7^{\circ}\text{C}$  and  $\sim 0.4^{\circ}\text{C}$ . The enhanced warming in 2018–2019 has caused a decrease in density ( $\sigma_t$ ) values of the LIW core, which gave way to the shallowest record of this water mass ( $\sim 110\text{-m}$  depth), bringing it well within the lower photic zone. We suggest that a higher level of nutrients became available, supporting the observed long-term rise of the intergraded chlorophyll *a* (Chl.*a*) ( $0.89\text{ mg m}^{-2}\text{ year}^{-1}$ ), with a maximum recorded during 2018–2019. The long-term record of the mixed layer depths shows no significant change; thus, the uplift of nutrients during winter mixing cannot support the trend and variations of the integrated Chl.*a*. Additional biological parameters of specific picoplankton populations and integrated bacterial production and abundance were measured in 2013–2021, but the measurements were too sparse to follow a clear interannual dynamics. Yet significantly higher average

levels for integrated primary production and bacterial abundances were observed during the anticyclonic period (as for Chl.a). The combined impacts of the BIOS mechanism and global warming, and hence the increase in LIW residence time and buoyancy, may impact the primary producers' biomass at the photic zone. This latter feedback may slightly counter the enhanced oligotrophication due to enhanced stratification.

#### KEYWORDS

Mediterranean Sea, thermohaline, water masses, Levantine, biochemical, nutrients, chlorophyll, phytoplankton

## Introduction

The Mediterranean Sea (MS) is dominated by an anti-estuarine thermohaline circulation driven by the salinity differences between the inflowing low-salinity Atlantic Water (AW) and mainly the outflowing highly saline Levantine intermediate water (LIW). The basin-scale circulation is broadly described in terms of a surface flow of AW from the Atlantic Ocean entering through the Strait of Gibraltar and proceeding to the eastern basin through the Strait of Sicily, and a return flow of LIW, originating in the Levantine Basin (LB), proceeding toward Strait of Gibraltar and finally exiting into the Atlantic (Tanhua et al., 2013; Malanotte-Rizzoli et al., 2014 and references therein).

Following early works on the surface circulation in the Eastern Mediterranean Sea (EMS) (Nielsen, 1912; Wust, 1961; Ovchinnikov, 1966; Bethoux, 1980), the observations achieved in the framework of the Physical oceanography of the Eastern Mediterranean (POEM) program (Malanotte-Rizzoli and Hecht, 1988) provided an important stepping stone in the understanding of the EMS circulation and yielded many studies elucidating on basin-scale circulation and sub-basin scale and mesoscale circulation patterns (Robinson et al., 1991; Ozsoy et al., 1991; POEM Group, 1992; Malanotte-Rizzoli et al., 1997). The resulting updated comprehensive description was of a set of sub-basin gyres connected by a system of jet currents (Robinson et al., 1991; Robinson and Golnaraghi, 1993). The AW coming into the EMS through the Sicily Channel follows an anticyclonic path through the southern Ionian, continuing thereon toward the Levantine to form the Mid-Mediterranean Jet, which flows from southwest to northeast in the center of the basin and joins the Asia Minor Current (Malanotte-Rizzoli et al., 1997). Later publications affirmed the previously described along-slope basin-wide circulation and gave attention to the unstable nature of the southern along-slope current developing anticyclonic eddies, which disperse part of the AW northward (Millot and Taupier-Letage, 2005; Hamad et al., 2006). In recent

years, a surface circulation scheme accommodating both the along-slope cyclonic circulation (as in Millot and Taupier-Letage, 2005) and the Mid Mediterranean Jet of Robinson and Golnaraghi (1993) was demonstrated for the EMS using drifter and altimetry data (Menna et al., 2012; Menna et al., 2020). Based on a high-resolution simulation for the period of 2011 to 2020, Estournel et al. (2021) described seasonal variations of the cyclonic, along-slope current as being stronger and more stable in winter, while in summer, it tends to be interrupted, and the continuity of the circulation is maintained by a train of eddies.

LIW formation occurs mainly in the Rhodes Gyre area (Lascaratos and Nittis, 1998; Lascaratos et al., 1999), yet compelling evidence is given to additional formation sources along the Turkish and Israeli coasts (Kubin et al., 2019; Fach et al., 2021), as well as the entire basin (Lascaratos et al., 1993; Ozsoy et al., 1993). An additional established source of intermediate water in the EMS is the South Aegean Sea producing the Cretan Intermediate water (CIW) (Georgopoulos et al., 1989; Schlitzer et al., 1991; Velaoras et al., 2014; Velaoras et al., 2019). LIW generally flows westward spreading from the Levantine Basin to the Ionian Basin (IB) and then through the Sicily Channel into the Western Basin, eventually exiting the MS through the Strait of Gibraltar below the AW layer (Lascaratos et al., 1999; Tanhua et al., 2013; Malanotte-Rizzoli et al., 2014). The pathways of LIW within the EMS have high variability but can be generally described as follows. LIW flow along the coast south of Crete, with part of the LIW flowing through the straits of the eastern Cretan Arc at intermediate depths into South Aegean to exit with the CIW through the western straits. The LIW flows in the Ionian bifurcates, one track circulating in the Ionian and the other headed toward the Sicily Channel (Malanotte-Rizzoli et al., 1999; Millot and Taupier-Letage, 2005). An additional important feature of the LIW flow feeds the Southern Adriatic Sea, introducing high-salinity masses into the Adriatic, and is considered to be a preconditioning factor for the formation of Adriatic Dense Water (Gacic et al., 2010; Gacic et al., 2011;

Schroeder et al., 2012). Seasonality in the LIW flow regime was recently presented (Pinaridi et al., 2019; Lyubartsev et al., 2020; Estournel et al., 2021; Menna et al., 2021) as well as their water mass properties in the East Mediterranean (Gacic and Bensi, 2020; Fedele et al., 2022 and references therein; Hayes et al., 2019). Estournel et al. (2021) outline the rim current of the Rhodes Gyre dispersing the LIW throughout the eastern Levantine in winter, while in summer, anticyclonic circulation that occupies the southeast of the basin redistributes LIW toward the south of the Levant. This LIW circulation of relatively high salinity and nutrient levels plays an important role in the deep-water formation in both the eastern and western basins (Robinson et al., 2001; Schneider et al., 2014) and the biogeochemistry of the MS (Malanotte-Rizzoli et al., 2014; Powley et al., 2014).

The LB is significantly influenced by the water exchange with the IB *via* the Cretan passage. The Adriatic–Ionian Bimodal Oscillating System (BiOS), thoroughly described in Gacic et al., 2011; Gacic et al. (2010 and experimentally by Rubino et al. (2020), controls the trajectory of the AW flow after passing through the Sicily Straits to both the Southern Adriatic (SA) and the LB, which correspond to quasi-decadal reversals in the North Ionian Gyre (NIG). The BiOS mechanism has been shown to have a significant effect on the physical and chemical dynamics in the SA (Civitarese et al., 2010; Gacic et al., 2010; Lavigne et al., 2018; Mihanovic et al., 2020; Menna et al., 2022; Placenti et al., 2022) as well as in the LB (Ozer et al., 2017). These studies proposed that the BiOS mechanism is a feedback mechanism between changes in the thermohaline structure of SA waters and the IB. In periods of cyclonic NIG, high-salinity LIW is injected into the SA, while the transport of AW is diverted to the LB. This results in buoyancy loss in the SA, which is thought to be a preconditioning factor for the formation of Adriatic Dense Water (Gacic et al., 2010; Gacic et al., 2011). During the anticyclonic NIG, AW intrusion into the Ionian and Adriatic Basins increases at the expense of the LB, and the formation of Adriatic Dense water is minimized. In accordance with these variations, Gacic et al. (2011) showed that during cyclonic NIG, surface salinity in the SA and IB increases and co-varies with nitrate levels in both the SA and IB in opposite phases (Civitarese et al., 2010). Ozer et al. (2017) described the magnitude of the long-term and superimposed thermohaline interannual variations and corresponding changes in nutrient and chlorophyll *a* (Chl.*a*) levels in the upper water masses of the LB (LSW and LIW), attributing them to the long-term climate change and the interannual BiOS mechanism, respectively.

The variability in physical and biogeochemical properties observed in the Mediterranean through the last few decades (Malanotte-Rizzoli et al., 2014; Von Schuckmann et al., 2020) calls for more systematic monitoring of this basin. Here we explore the relationships between the interannual variations of the LIW thermohaline properties and its vertical position with the corresponding biochemical variations in the euphotic zone

(e.g., integrated nutrients, alkalinity, dissolved oxygen, Chl.*a*, picoplankton populations, and primary and bacterial production) at the Southeastern Mediterranean Sea. For this purpose, we make use of data collected in three deep-water stations (1,100–1,600 m) in the eastern LB, which was visited two to three times annually. The thermohaline and Chl.*a* datasets represent ~20 years (2002–2021), while the additional biological data represent the last 9 years (2013–2021). We use Mediterranean Sea Physical Reanalysis data (Escudier et al., 2020; [https://doi.org/10.25423/CMCC/MEDSEA\\_MULTIIYEAR\\_PHY\\_006\\_004\\_E3R1](https://doi.org/10.25423/CMCC/MEDSEA_MULTIIYEAR_PHY_006_004_E3R1)) to examine the relationship of our findings to variations of the mixed layer depths (MLDs) and the volume of AW in the southeastern MS. Recent results (Fedele et al., 2022; Menna et al., 2022) support the advantage of using LIW to describe the long-term warming and salinization and the interannual BiOS mechanism, which is less sensitive to the seasonal cycle but is yet shallow enough to reflect surface layer and photic zone dynamics.

## Materials and methods

### Sampling/cruise data

The presented data are composed mostly of new 17 Haifa Section (HaiSec) cruises extending 90 km to the northwest of the Carmel Headland, northern Israel, which were conducted during the period 2013–2021, including only deep stations H04, H05, and H06 (>1,000-m water depth) (Figure 1). Additional data from previous years (since 2002) at the same stations are included (Ozer et al., 2017), as well as 10 CTD casts at station H05. All surveys were carried out by the Israel Oceanographic and Limnological Research Institute (IOLR). The cruises were conducted aboard the *R/V Shikmona* until 2015 and since 2016 aboard the new Israeli *R/V Bat-Galim*. A Sea-Bird SBE911plus CTD system, interfaced to an SBE Carousel, was used to collect continuous profiles (24 Hz) of pressure, temperature, salinity, dissolved oxygen, and fluorescence. The manufacturer reported that the precision of the SBE911plus CTD is  $\pm 0.0025$  for salinity (inferred from the  $\pm 0.0003$  S/m conductivity precision) and  $\pm 0.001^\circ\text{C}$  for temperature. Throughout the period covered by this dataset, the pressure, conductivity, and temperature sensors were calibrated by the manufacturer periodically every 2 years (as described in Ozer et al., 2020). CTD data were processed using the Sea-Bird data processing software following the manufacturer's recommendations. The CTD data validation procedure included lowering an additional autonomous SBE19/SBE19plus CTD (factory calibrated within the last year) parallel to the onboard SBE9plus in order to obtain duplicate casts, ensuring that any non-conformities remained within the sensors' precision. Samples of dissolved oxygen and Chl.*a* (described below) were used to calibrate the dissolved oxygen profiles from the CTD.

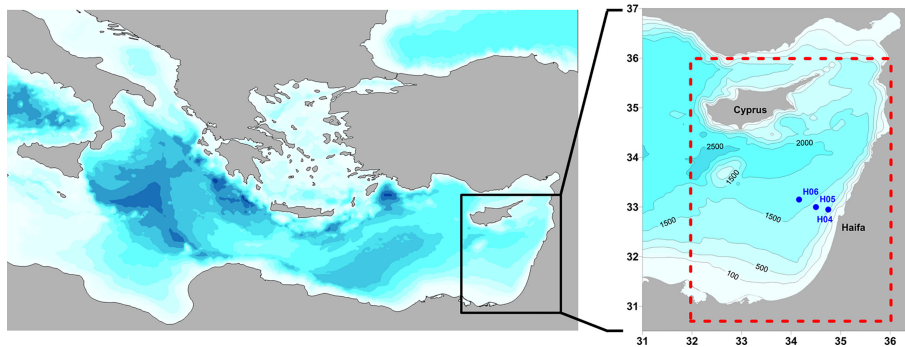


FIGURE 1

Map of hydrographic stations visited during the IOLR Haifa Section deep stations (blue dots, performed biannually). Station H05 was additionally visited in 10 cruises. Domain of CMEMS physical reanalysis used for MLD, and AW volume estimate is marked by the dotted red rectangle. IOLR, Israel Oceanographic and Limnological Research Institute; CMEMS, Copernicus Monitoring Environment Marine Service; MLD, mixed layer depth; AW, Atlantic Water.

## Atlantic water volume and mixed layer depth variability

The products of monthly salinity, potential temperature, and MLD from the MS physical reanalysis provided by the E.U. Copernicus Monitoring Environment Marine Service (CMEMS) (Escudier et al., 2020) were obtained for the southeastern MS (30.7° to 36°N and 32° to 36.2°E, Figure 1) for the period of January 2002 to May 2020. The reanalysis data had a horizontal grid resolution of 1/24° (ca. 4–5 km) and 141 unequally spaced vertical levels. The MLD data were averaged over the complete domain in order to eliminate the sensitivity of the data to mesoscale activity and attain a general estimate for this part of the basin.

In order to quantify the volume of AW, we performed a volumetric statistical analysis (VSA) introduced by Cochran (1958); Montgomery (1958), and Pollak (1958) and more recently used for the Aegean by Gertman et al. (2006). This approach is based on assigning temperature (>15°C) and salinity (<38.9) ranges, which are considered to be characteristic of AW. For each time step of the reanalysis model, the volume occupied by AW (where thermohalines values match those of AW characteristics) is summed up over the entire domain, and its percentage of the domain is calculated. In order to achieve this, we first calculated the volume (in m<sup>3</sup>) of each data point, considering the spatial and vertical distribution of the data, as follows:

$$V_{lat,lon,z} = dlat * dlon * |Z_{(i+1)} - Z_{(i-1)}| / 2$$

where  $V$  is the volume of a specific grid point in m<sup>3</sup>;  $dlat$  and  $dlon$  are the constant latitude and longitude distances of 4,620, and 4,010 m, respectively;  $Z$  is the depth level in meters. Next, a matrix of potential temperature and salinity ( $\theta$ - $S$  space) was created with the ranges of 13°C to 30°C with a 0.1°C interval for

temperature and 37.8 to 39.5 with a 0.01 interval for salinity, representing the complete range of thermohaline values found in the dataset. The reanalysis data were then filtered through, and the volume of each data point was accumulated in the relevant  $\theta$ - $S$  space position, based on its rounded temperature and salinity values. For the evaluation of the total AW volume in the domain, we summed up all the matrix cells with temperatures above 15°C and salinities below 38.9, and finally, we calculated the percentage of the domain volume occupied by AW for each time step (i.e., month). The choice of these threshold values can be contested, mainly for salinity, thus changing the total volumes achieved through this method. For this reason, several iterations, with the salinity limit ranging from 38.85 to 39.95 (with 0.01 interval), were tested and gave similar trends (not presented). Thus, we considered these results to be a strong proxy for the overall volume of AW in the Levant basin, so that the variability is well presented, not the absolute volume values.

## Levantine intermediate water and photic zone investigation

In order to minimize the effects of mesoscale phenomena on our analysis, we only examined the core values of LIW, which are less affected by diapycnal mixing and more controlled by isopycnal processes. The vertical position of the LIW core was identified by finding the maximal salinity value of each cast within the depth range of intermediate water (100 and 350 m; Ozer et al., 2017). Subsequently, the physical and chemical data of the LIW core depth were averaged for all the stations of each cruise, and finally, the resultant time series was smoothed, using a moving average with a time window of 1 year. Additionally, the contemporaneous biological parameters were integrated over the photic zone (0–200 m) using water column sampling and

analyses, while the Chl.*a* profiles and integrated values were obtained from the calibrated CTD fluorescence measurements.

## Dissolved oxygen, alkalinity, and inorganic nutrients analysis

Water samples for dissolved oxygen and inorganic nutrients were collected at sampling depths based on the thermohaline structure of the water column, representing the different water masses. Water samples for dissolved oxygen were sampled and measured in duplicates onboard immediately after sampling following the modified Winkler method (Carpenter–Winkler titration procedure [Carpenter, 1965](#)), using an automated Metrohm Titrando 905 titration system. Duplicate samples for nutrient analysis were collected in 15-ml acid-washed plastic scintillation vials and immediately frozen.

Total alkalinity (TA) was measured by potentiometric titration with a Metrohm, 848 Titrino plus system using the Gran method to calculate it from acid volumes and corresponding pH measurements between pH 3.3 and 3.8 ([Ben-Yaakov and Sass, 1977](#)). The titration acid was 0.05 M of HCl, which was verified and adjusted using certified reference seawater supplied by the Certified Reference Materials Laboratory, Scripps Institution of Oceanography, CA ([Dickson et al., 2003](#)). Duplicate measurements were made for each sample, and the precision error was  $\pm 1 \mu\text{mol kg}^{-1}$ .

Nutrients were measured with a Seal Analytical AA-3 system ([Sisma-Ventura et al., 2022](#)). The limits of detection (LODs), estimated as three times the standard deviation of 10 measurements of the blank (low nutrient aged seawater collected from the off-shore surface at the Levantine Basin) for  $\text{PO}_4$ ,  $\text{Si}(\text{OH})_4$ ,  $\text{NO}_2+\text{NO}_3$  ( $\text{NO}_x$ ), and  $\text{NH}_4$ , were 8, 80, 80, and 90 nM, respectively. The reproducibility of the analyses was determined using certified reference materials (CRMs): MOOS 3 ( $\text{PO}_4$ ,  $\text{NO}_x$ ,  $\text{NH}_4$ , and  $\text{Si}(\text{OH})_4$ ), VKI 4.1 ( $\text{NO}_x$ ), and VKI 4.2 ( $\text{PO}_4$  and  $\text{Si}(\text{OH})_4$ ). The sample analysis results were accepted when measured CRMs were within  $\pm 5\%$  of the certified values. Quality control of the nutrient measurements over the years was performed with the use of internal and certified reference standards and by participation in international laboratory performance exercises (QUASIMEME).

## Biological analyses

Seawater samples (500 ml) for chlorophyll *a* determination were filtered through GF/F filters that were then wrapped in aluminum foil and frozen ( $-20^\circ\text{C}$ ). At the lab, the chlorophyll *a* pigment was extracted from the filters using acetone (90%) overnight and determined by the non-acidification method ([Welschmeyer, 1994](#)) using a Turner Designs (Trilogy) fluorometer.

Pico-phytoplankton abundance was determined by flow cytometry. Briefly, seawater samples (1.8 ml) were fixed with glutaraldehyde (0.02% v:v, Sigma-Aldrich, St. Louis, MO, USA; G7651) at room temperature for 10 min and frozen in liquid nitrogen. The abundance of autotrophic pico-eukaryotes, *Synechococcus* and *Prochlorococcus*, was determined using an Attune<sup>®</sup> Acoustic Focusing Flow Cytometer (Applied Biosystems, Foster City, CA, USA).

Primary productivity was determined following the [Steemann Nielsen \(1952\)](#) protocol. Specifically, triplicate water samples from each depth (50 ml) were spiked with 5  $\mu\text{Ci}$  of  $\text{NaH}^{14}\text{CO}_3$  (PerkinElmer, Waltham, MA, USA; specific activity 56 mCi  $\text{mmol}^{-1}$ ) and incubated for 24 h under *in situ* natural illumination and temperature in a flow-through tank on deck. Measurements for the added activity and dark controls were also performed. The incubations were terminated by filtering the seawater through GF/F filters and acidifying them overnight in 5-ml scintillation vials containing 50  $\mu\text{l}$  of 32% hydrochloric acid to remove excess  $^{14}\text{C}$ . Lastly, 5 ml of an Ultima-Gold scintillation was added to the filters, and the radioactivity was measured using a TRI-CARB 2100 TR (Packard) liquid scintillation counter.

For measurements of bacterial abundance, heterotrophic bacteria were stained (300  $\mu\text{l}$  of the initial sample) with SYBR Green Fluorescent Nucleic Acid Stain (Applied Biosystems) and enumerated by discrimination based on green fluorescence (530 nm) and side scatter ([Marie et al., 1997](#)). Bacterial production was estimated using the  $^3\text{H}$ -leucine incorporation method. Triplicate samples (1.7 ml) were incubated with  $\sim 100$  nmol hot leucine  $\text{L}^{-1}$  for 4–7 h (PerkinElmer; specific activity 100 Ci  $\text{mmol}^{-1}$ ). ‘Kill’ treatments in which seawater was added with 100  $\mu\text{l}$  of 100% trichloroacetic acid (TCA;  $4^\circ\text{C}$ ) along with  $^3\text{H}$ -leucine were also carried in triplicates from representing depths (surface water was usually used). The incubations were terminated with TCA and were later processed following the micro-centrifugation technique ([Smith et al., 1992](#)) and added with 1 ml of an Ultima-Gold scintillation cocktail. The samples were counted using a TRI-CARB 2100 TR (Packard) liquid scintillation counter. A conversion factor of 1.5 kg C  $\text{mol}^{-1}$  per mol leucine incorporated was used ([Simon et al., 1989](#)).

## Results and discussion

The averaged salinity and temperature time series of the LIW core present a good agreement with the presiding circulation pattern of the north Ionian, the BiOS mechanism ([Civitarese et al., 2010](#); [Gacic et al., 2010](#); [Lavigne et al., 2018](#); [Menna et al., 2022](#); [Placenti et al., 2022](#)). Periods of anticyclonic circulation (tinted in red in [Figure 2](#)) are characterized by a positive tendency in salinity and temperature, while cyclonic periods (tinted in blue) are accompanied by a decrease in the thermohaline values of LIW. In our display ([Figures 2–4](#), [Supplementary Figure S1](#)), we extend the final cyclonic period starting in 2019 ([Menna et al., 2022](#)) through the end of the

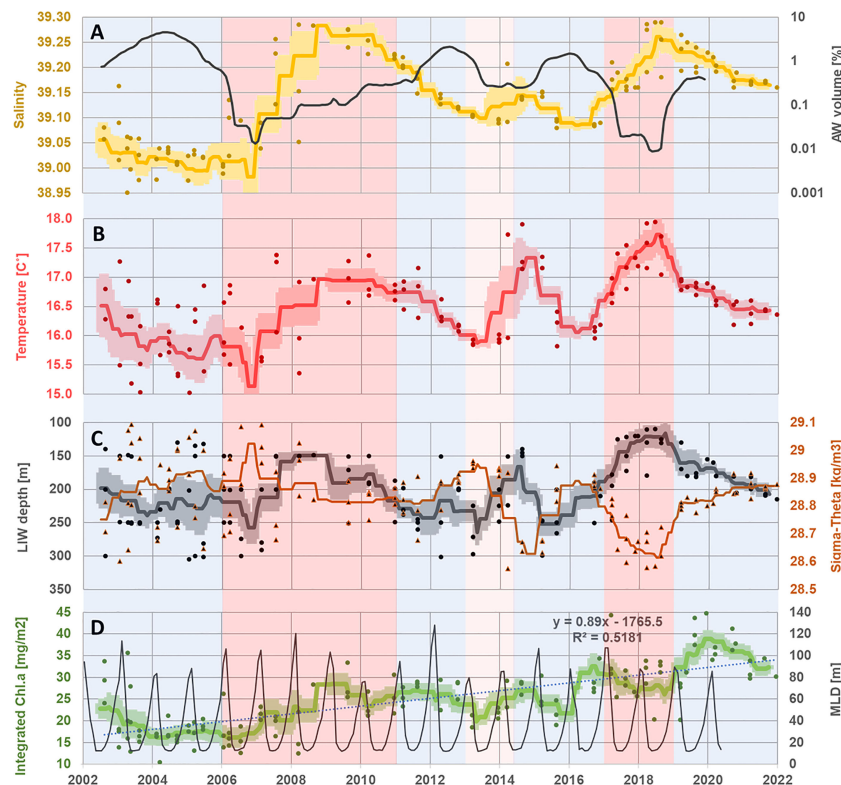


FIGURE 2

Time series of salinity (A; yellow), Atlantic Water volume percentage (A; black), temperature (B; red), depth (C; black), density (Sigma-Theta; C; orange), and mixed layer depth (MLD; D; black) performed in the core of the LIW water mass (ca. 130 m <math>z</math> <math>< 350</math> m) during the Haifa Section cruises (2002–2021). Time series of integrated chlorophyll *a* at the photic zone (0–200 m) (D; green). Station-specific values are presented in dots, the moving average is presented in a solid line, and the standard error ranges are indicated with a light-colored area. Light blue dotted line and formula show the calculated chlorophyll *a* trend. Periods of anticyclonic circulation (tinted in red in the salinity panel) and cyclonic periods (tinted in blue) (Menna et al., 2022; Placenti et al., 2022).

presented time series, as our data support it with the continuation of a negative trend in thermohaline values. The long-term warming and salinification trends are clearly evident in the presented data in agreement with previously published studies (Ozer et al., 2017; Ozer et al., 2022). The annual average LIW core depth varies from 130 to 270 m (average values) over the examined period were mostly affected by the density (Sigma-Theta) values of this water mass (Pearson's correlation value of 0.6). This relationship is most evident in 2018, where LIW core reached a record low of sigma of  $\sim 28.6$  kg  $m^{-3}$ , while its average core depth decreased significantly and reached  $\sim 110$  m (annual average 130 m) (Figure 2), the shallowest depth recorded here along the 20 years' time series (2002–2021). It should be noted that although the LIW reached a high-salinity content at this time (2018), which is similar to the 2008 salinity peak, it has reached a maximal temperature value of 17.7°C, attributed to the long-term warming trend, permitting a minimal density as described above.

The AW volume variability, as achieved through the VSA, closely follows the cyclonic–anticyclonic regime of the north Ionian as described thoroughly by Menna et al. (2022). In the periods of anticyclonic circulation, when the water exchange in

the Levant is reduced according to the BiOS theory (Gacic et al., 2010), there is indeed a significant reduction in the volume of AW in the EMS by up to two orders of magnitude. The opposite occurs in reported periods of cyclonic circulation in the north Ionian, which are characterized by high AW volume. The AW VSA results are also in the opposite phase of the LIW salinity time series, providing important evidence of the link between the variability of the Ionian circulation to the water fluxes coming in and out of the LB and through this mechanism influencing the thermohaline and nutrient values of the LIW.

The total alkalinity concentrations (Supplementary Figure S1) are in accord with concentrations recorded in the Mediterranean Sea ( $\sim 2,600$   $\mu\text{mol kg}^{-1}$ ), showing relatively high levels (Kolker et al., 2021). We observed a peak in the total alkalinity concentration coinciding with the 2018 salinity peak (Supplementary Figure S1), yet the existing data for 2013–2021 are too small to draw a firm behavior and display concentrations, which follow the conservative behavior (linear trend) of total alkalinity with salinity (Kolker et al., 2021, and references therein).

Dissolved oxygen values correspond closely with the LIW core depth and can be related to enhanced ventilation of this water mass, as it becomes shallower and has higher oxygen demand due to organic material decomposition as it becomes deeper (Figure 3). The apparent oxygen utilization (AOU) time series behaves out of phase with the nutrient concentrations (Figure 3), reflecting the degree of organic matter degradation/oxidation. In addition, the nutrients ( $\text{NO}_3+\text{NO}_2$  and  $\text{PO}_4$ ) time series (Figures 3C) present a mirror image of the thermohaline and LIW depth data (Figures 2, 3), as they are presumably depleted from the LIW water mass when it becomes shallower and more available for primary production and is then replenished when LIW core deepens.

The integrated Chl.*a* time series also presents a general long-term positive trend. We observe a significant long-term rise in the integrated Chl.*a* of  $0.89 \text{ mg m}^{-2} \text{ year}^{-1}$  for the years 2002 till 2021 (Figure 2), superimposed by interannual variations. At three distinct times at the start of a shallowing period of the LIW core, at the beginning of 2007, the end of 2013, and the middle of 2016, there is a clear rise of the integrated Chl.*a* levels in the

photic zone (Figures 2, 3). The Chl.*a* time series partly coincides with the periods of anticyclonic and cyclonic circulations, not always in union with the thermohaline exact peaks and lows, demanding further investigation. The maximal winter MLD values from the CMEMS physical reanalysis product do not seem to correspond with the observed integrated Chl.*a* variations or its general increasing trend (Figure 2). Therefore, the supply of nutrients from deeper water due to the annual deep winter mixing does not support the general increasing trend and interannual variability of the integrated Chl.*a*.

The rise in the buoyancy of LIW core in 2018–2019 through its reduced sigma value gave way to the shallowest record of this water mass (~110-m depth), bringing it well within the lower photic zone. The LIW core in 2018–2019 is shallower by ~50 m as compared to the 2008–2010 peak (Figure 2) and as expected shows lower AOU values at the shallower depth (Figure 3). Nevertheless, in contrast to the expected AOU behavior, both periods contain similar concentrations of  $\text{NO}_3$ , showing relatively enriched concentrations in the 2018–2019 LIW core (Figure 3). Thus, the mechanism of warming and shallowing the

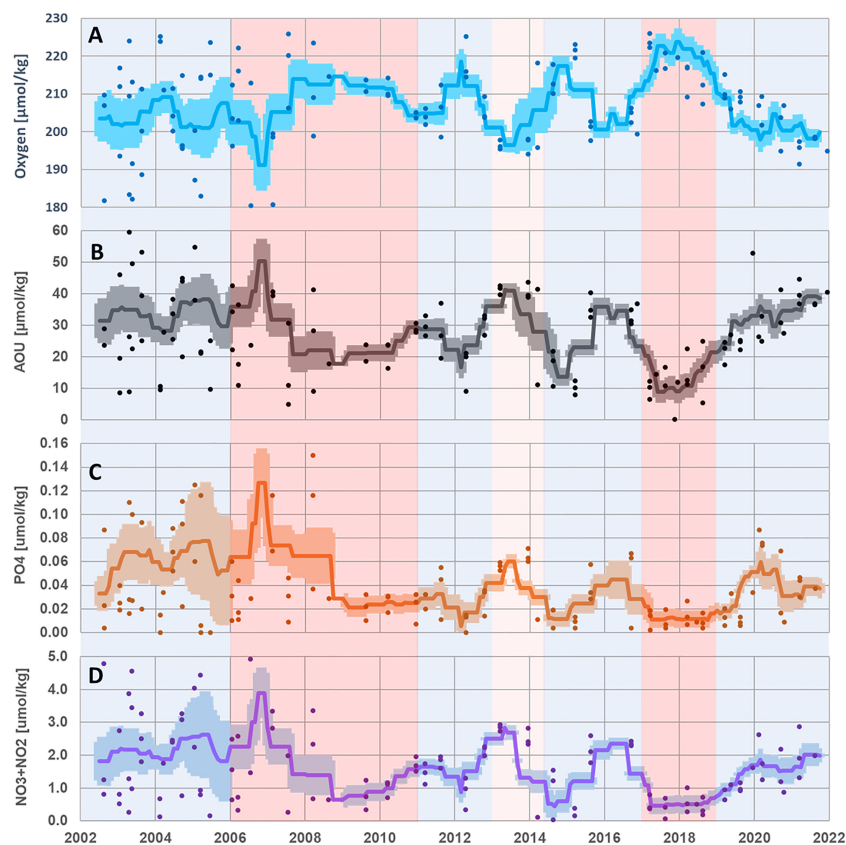


FIGURE 3

Time series of dissolved oxygen (A; blue), Apparent oxygen utilization (AOU; B; black), dissolved  $\text{PO}_4$  concentrations (C; orange), and dissolved  $\text{NO}_3+\text{NO}_2$  concentrations (D; purple) were performed in the core of the LIW water mass (ca.  $130 \text{ m} < z < 350 \text{ m}$ ) during the Haifa Section cruises (2002–2021). Station-specific values are presented in dots; the moving average is presented in a solid line, and the standard error ranges are indicated with a light-colored area. Circulation periods are presented as in Figure 2. LIW, Levantine intermediate water.

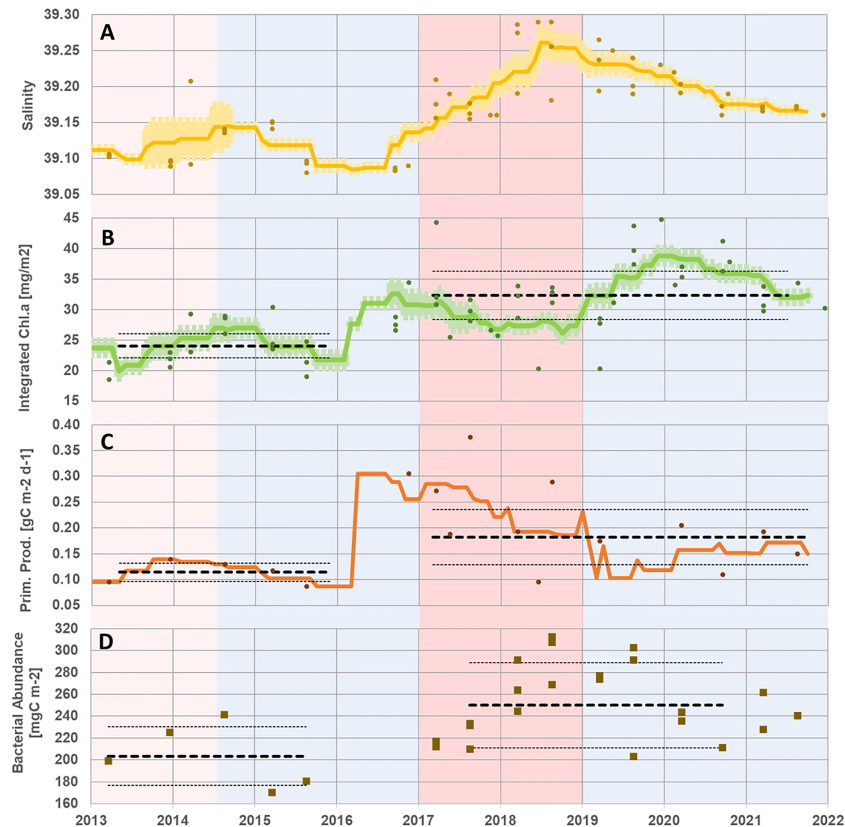


FIGURE 4

Time series of salinity (A; yellow) as presented in Figure 1 for the 2013–2021 time slot and time series of integrated Chl.a (B; green), integrated primary production (C; orange), and integrated bacterial production (D; brown) performed at the photic zone (0–200 m) during the Haifa Section cruises (2013–2021). Station-specific values are presented in dots, the moving average is presented in a solid line, and the standard error ranges are indicated with a light-colored area (for salinity and Chl.a). The bold black segmented lines and the thin dotted side lines in panels (C) and (D) represent the average and standard deviation range, respectively. Circulation periods are presented as in Figure 2.

LIW core due to its increased buoyancy enabled a higher level of nutrients to become available to the photic zone from below, supporting the observed rise of the integrated Chl.a (or algae biomass), with a maximum recorded during 2018–2019. Accordingly, we further suggest that this mechanism of warming and shallowing the LIW core may explain the general long-term rise of the integrated Chl.a (Figure 2) as the LIW core becomes gradually more available for photosynthetic activity.

The 2013–2021 time series shows two distinct periods of BiOS, mainly cyclonic (2011–2016; Placenti et al., 2022) and mostly anticyclonic (2017–2019; Menna et al., 2022). It is expected that the biological response to BiOS is complex and exhibits certain delay and thus does not coincide with the detailed thermohaline interannual variations. Pearson lag correlations for the above time series presented maximal values of  $\sim 0.82$  with the integrated Chl.a lagging  $\sim 22$  months behind the thermohaline parameters, attesting to the

delayed response of the biological cycle to the observed physical changes in LIW core properties. Nonetheless, considering the above two general periods, a significant ( $p < 0.05$ ) change in the average integrated values for primary production and bacterial abundance (as for Chl.a) shows higher levels after 2017, during the anticyclonic period and afterward (Figure 4). Other integrated biological parameters measured during this period are too sparse to follow detailed interannual variations (Supplementary Figure S1). Specifically, data on the abundance of pico-phytoplankton populations (autotrophic pico-eukaryotes, *Synechococcus* and *Prochlorococcus*) and integrated bacterial production were too sparse, preventing any clear statistical significance (Supplementary Figure S1). Further observations are required to better assess the response of such pico-phytoplankton populations.

The changes in buoyancy, consequent of the changes in the thermohaline values, are the main mechanism controlling the

vertical position of LIW in the SE Levantine Basin. The vertical uplift of the nutrient-rich LIW water is an important and significant pathway of nutrients into the photic zone driving the primary production in this oligotrophic area, especially during anticyclonic periods, which prolong the residence time of the LIW due to its reduced outflow from the LB. Thus, global warming in combination with the BiOS mechanism, and hence LIW residence time and buoyancy, may impact the primary producers' biomass at the photic zone and hence somewhat reduce the degree of oligotrophic state. This latter feedback may slightly counter the enhanced oligotrophication due to the warming effect on enhanced stratification and mixing depths. Further observations are needed to better understand and assess these processes.

## Data availability statement

The datasets presented in this study can be found in online repositories (physical updated and chemical in process). The names of the repository/repositories and accession number(s) can be found at: Israel Marine Data Center—<https://isramar.ocean.org.il/isramar2009/>.

## Author contributions

Conceptualization: BH and TO. Data acquisition: TO, IG, ER, GS-V, BH, and JS. Formal analysis: TO, IG, ER, GS-V, JS, and BH. Project administration: BH. Writing—original draft: TO and BH with the help of IG, ER, GS-V, and JS. All authors approved the submitted version.

## Funding

This study was supported by the Israel Ministries of Energy and Environmental Protection through the National Monitoring Program of Israel's Mediterranean waters.

## References

- Ben-Yaakov, S., and Sass, E. (1977). Independent estimate of the PH of dead Sea brines, *limnol. Oceanogr.* 22, 374–376. doi: 10.4319/lo.1977.22.2.0374
- Bethoux, J. P. (1980). Mean water fluxes across sections in the Mediterranean Sea, evaluated on the basis of water and salt budgets and of observed salinities. *Oceanologica Acta* 3, 79–88.
- Carpenter, J. H. (1965). The accuracy of the winkler method for dissolved oxygen analysis. *Limnology Oceanography* 10, 135–140. doi: 10.4319/lo.1965.10.1.0135
- Civitaresse, G., Gacic, M., Lipizer, M., and Borzelli, G. L. E. (2010). On the impact of the bimodal oscillating system (BiOS) on the biogeochemistry and biology of the Adriatic and Ionian seas (Eastern Mediterranean). *Biogeosciences* 7, 3987–3997. doi: 10.5194/bg-7-3987-2010

## Acknowledgments

We thank the captain and crew of the *R/V Bat-Galim* operated by the Israel Oceanographic and Limnological Research Institute (IOLR). We thank the maritime crew, electrical lab, and research assistants at the physical oceanography, marine chemistry, and biology departments at IOLR for their dedicated efforts.

## Conflict of interest

The authors declare that the research was conducted in the absence of any commercial or financial relationships that could be construed as a potential conflict of interest.

## Publisher's note

All claims expressed in this article are solely those of the authors and do not necessarily represent those of their affiliated organizations, or those of the publisher, the editors and the reviewers. Any product that may be evaluated in this article, or claim that may be made by its manufacturer, is not guaranteed or endorsed by the publisher.

## Supplementary material

The Supplementary Material for this article can be found online at: <https://www.frontiersin.org/articles/10.3389/fmars.2022.958924/full#supplementary-material>

### SUPPLEMENTARY FIGURE 1

Time series of alkalinity (A, red), *Synechococcus* (B, blue), *Prochlorococcus* (C, orange) pico-eukaryotes (D, green) and integrated bacterial production (E, grey) performed at the photic zone (0–200m) during the Haifa Section cruises (2013–2021). Station-specific values are presented in dots and the moving average is presented in a solid line. Circulation periods are presented as in Figure 2.

- Cochrane, J. D. (1958). The frequency distribution of water characteristics in the Pacific ocean. *Deep-Sea Res.* 5, 111–127. doi: 10.1016/0146-6313(58)90002-9

- Dickson, A. G., Afghan, J. D., and Anderson, G. C. (2003). Reference materials for oceanic CO<sub>2</sub> analysis: a method for the certification of total alkalinity. *Mar. Chem.* 80, 185–197. doi: 10.1016/S0304-4203(02)00133-0

- Escudier, R., Clementi, E., Omar, M., Cipollone, A., Pistoia, J., Aydogdu, A., et al. (2020). *Mediterranean Sea Physical reanalysis (CMEMS MED-currents) (Version 1) [Data set]* (Copernicus Monitoring Environment Marine Service (CMEMS)). doi: 10.25423/CMCC/MEDSEA\_MULTITYEAR\_PHY\_006\_004\_E3R1

- Estournel, C., Marsaleix, P., and Ulses, C. (2021). A new assessment of the circulation of Atlantic and intermediate waters in the Eastern Mediterranean. *Prog. Oceanography* 198, 102673. doi: 10.1016/j.pocan.2021.102673

- Fach, B. A., Orek, H., Yilmaz, E., Tezcan, D., Salihoglu, I., Salihoglu, B., et al. (2021). Water mass variability and levantine intermediate water formation in the Eastern Mediterranean between 2015 and 2017. *J. Geophysical Research: Oceans* 126, e2020JC016472. doi: 10.1029/2020JC016472
- Fedele, G., Mauri, E., Notarstefano, G., and Poulain, P.-M. (2022). Characterization of the Atlantic Water and levantine intermediate water in the Mediterranean Sea using 20 years of argo data. *Ocean Sci.* 18, 129–142. doi: 10.5194/os-18-129-2022
- Gacic, M., and Bensi, M. (2020). Ocean exchange and circulation. *Water* 12 (2020), 882. doi: 10.3390/w12030882
- Gacic, M., Borzelli, G. L. E., Civitarese, G., Cardin, V., and Yari, S. (2010). Can internal processes sustain reversals of the ocean upper circulation? the Ionian Sea example. *Geophys. Res. Lett.* 37, L09608. doi: 10.1029/2010GL043216
- Gacic, M., Civitarese, G., Eusebi Borzelli, G. L., Kovacevic, V., Poulain, P.-M., Theocharis, A., et al. (2011). On the relationship between the decadal oscillations of the northern Ionian Sea and the salinity distributions in the Eastern Mediterranean. *J. Geophys. Res.* 116, C12002. doi: 10.1029/2011JC007280
- Georgopoulos, D., Theocharis, A., and Zodiatis, G. (1989). Intermediate water formation in the Cretan Sea (South Aegean Sea). *Oceanologica Acta* 12 (4), 353–359.
- Gertman, I., Pinardi, N., Popov, Y., and Hecht, A. (2006). Aegean Sea Water masses during the early stages of the Eastern Mediterranean climatic transition (90). *J. Phys. Oceanography* 36 (9), 1841–1859. doi: 10.1175/JPO2940.1
- Hamad, N., Millot, C., and Taupier-Letage, I. (2006). The surface circulation in the Eastern basin of the Mediterranean Sea. *Scientia Marina* 70, 457–503. doi: 10.3989/scimar.2006.70n3457
- Hayes, D., Poulain, P.-M., Testor, P., Mortier, L., Bosse, A., and Du Madron, X. (2019). Review of the circulation and characteristics of intermediate water masses of the Mediterranean—implications for cold-water coral habitats. *Coral reefs Mediterr. (CORM)* 9, f1hal-02400788. doi: 10.1007/978-3-319-91608-8\_18
- Kolker, D., Bookman, R., Herut, B., David, N., and Silverman, J. (2021). An initial assessment of the contribution of fresh submarine ground water discharge to the alkalinity budget of the Mediterranean Sea. *J. Geophysical Research: Oceans* 126 (8), e2020JC017085. doi: 10.1029/2020JC017085
- Kubin, E., Poulain, P.-M., Mauri, E., Menna, M., and Notarstefano, G. (2019). Levantine intermediate and levantine deep water formation: An argo float study from 2001 to 2017. *Water* 11, 1781. doi: 10.3390/w11091781
- Lascazatos, A., and Nittis, K. (1998). A high-resolution three-dimensional numerical study of intermediate water formation in the levantine Sea. *J. Geophys. Res.* 103 (C9), 18497–18511. doi: 10.1029/98JC01196
- Lascazatos, A., Roether, W., Nittis, K., and Klein, B. (1999). Recent changes in deep water formation and spreading in the Mediterranean Sea: A review. *Prog. Oceanography* 44, 5–36. Pergamon. doi: 10.1016/S0079-6611(99)00019-1
- Lascazatos, A., Williams, R. G., and Tragou, E. (1993). A mixed-layer study of the formation of levantine intermediate water. *J. Geophys. Res.* 98 (C8), 739–749. doi: 10.1029/93JC00912
- Lavigne, H., Civitarese, G., Gačić, M., and D'Ortenzio, F. (2018). Impact of decadal reversals of the north Ionian circulation on phytoplankton phenology. *Biogeosciences* 15, 4431–4445. doi: 10.5194/bg-15-4431-2018
- Lyubartsev, V., Borile, F., Clementi, E., Masina, S., Drudi, M., Coppini, G., et al. (2020). Interannual variability in the Eastern and Western Mediterranean overturning index. in: Copernicus marine service ocean state report, issue 4. *J. Operational Oceanography* 13:sup1, s88–s91. doi: 10.1080/1755876X.2020.1785097
- Malanotte-Rizzoli, P., Manca, B.B., Ribera d'Alcala, M., Theocharis, A., Bergamasco, A., Bregant, D., et al. (1997). A synthesis of the Ionian Sea hydrography, circulation and water mass pathways during POEM-Phase I. *Prog. Oceanogr.* 39, 153–204. doi: 10.1016/S0079-6611(97)00013-X
- Malanotte-Rizzoli, P., and Hecht, A. (1988). Large-Scale properties of the Eastern Mediterranean: a review. *Oceanologica Acta* 11, 4.
- Malanotte-Rizzoli, P., Manca, B. B., d'Alcala, M., Theocharis, A., et al. (1997). A synthesis of the Ionian Sea hydrography, circulation and water mass pathways during POEM-phase I. *Prog. Oceanogr.* 39, 153–204. doi: 10.1016/S0079-6611(97)00013-X
- Malanotte-Rizzoli, P., Manca, B. B., Ribera, d'Alcala, M., Theocharis, A., Brenner, S., et al. (1999). The Eastern Mediterranean in the 80s and in the 90s: the big transition in the intermediate and deep circulations. *Dynamics Atmospheres Oceans* 29, 365–395. doi: 10.1016/S0377-0265(99)00011-1
- Marie, D., Partensky, F., Jacquet, S., and Vulot, D. (1997). Enumeration and cell cycle analysis of natural populations of marine picoplankton by flow cytometry using the nucleic acid stain SYBR green I. *Appl. Environ. Microbiol.* 63, 186–193. doi: 10.1128/aem.63.1.186-193.1997
- Menna, M., Gačić, M., Martellucci, R., Notarstefano, G., Fedele, G., Mauri, E., et al. (2022). Climatic, decadal, and interannual variability in the upper layer of the Mediterranean Sea Using remotely sensed and *In-situ* data. *Remote Sens.* 14(2022), 1322. doi: 10.3390/rs14061322
- Menna, M., Gerin, R., Notarstefano, G., Mauri, E., Bussani, A., Pacciaroni, M., et al. (2021). On the circulation and thermohaline properties of the Eastern Mediterranean Sea. *Front. Mar. Sci.* 8. doi: 10.3389/fmars.2021.671469
- Menna, M., Notarstefano, G., Poulain, P.-M., Mauri, E., Falco, P., and Zambianchi, E. (2020). Surface picture of the levantine basin as derived by drifter and satellite data, section 3.5 of von schuckmann et al. 2020. Copernicus Mar. Service Ocean State Rep. *J. Operational Oceanography* 4, S1–S172. doi: 10.1080/1755876X.2020.1785097
- Menna, M., Poulain, P.-M., Zodiatis, G., and Gertman, I. (2012). On the surface circulation of the levantine sub-basin derived from Lagrangian drifters and satellite altimetry data. *Deep-Sea Res. I* 65, 46–58. doi: 10.1016/j.dsr.2012.02.008
- Mihanovic' H, Vilibic' I, Šepic' J, Matic' F, Ljubecic' Z, Mauri, E., Gerin, R., et al. (2021). Observation, preconditioning and recurrence of exceptionally high salinities in the Adriatic Sea. *Front. Mar. Sci.* 8. doi: 10.3389/fmars.2021.672210
- Millot, C., and Taupier-Letage, I. (2005). "Circulation in the Mediterranean Sea," in *The handbook of environmental chemistry 5 (K)*. Ed. A. Salio (Springer-Verlag, Heidelberg), 29–66. doi: 10.1007/b107143
- Montgomery, R. B. (1958). Water characteristics of Atlantic ocean and of world ocean. *Deep-Sea Res.* 5, 134–148. doi: 10.1016/0146-6313(58)90004-2
- Nielsen, J. N. (1912). Hydrography of the Mediterranean and adjacent waters. *Rep. Dan. Oceanogr. Exped.* 1908–1910, 77–192.
- Ovchinnikov, M. (1966). Circulation in the surface and intermediate layers of the Mediterranean Sea. *Oceanology* 6, 48–59.
- Ozer, T., Gertman, I., and Gildor, H. (2022). Thermohaline temporal variability of the SE Mediterranean coastal waters (Israel) -long-term trends, seasonality, and connectivity. *Front. Mar. Sci.* 8, 799457. doi: 10.3389/fmars.2021.799457
- Ozer, T., Gertman, I., Gildor, H., Goldman, R., and Herut, B. (2020). Evidence for recent thermohaline variability and processes in the deep water of the southeastern levantine basin, Mediterranean Sea. *Deep Sea Res. Part II: Topical Stud. Oceanography* 171, 104651.
- Ozer, T., Gertman, I., Kress, N., Silverman, J., and Herut, B. (2017). Interannual thermohaline, (1979–2014) and nutrient, (2002–2014) dynamics in the levantine surface and intermediate water masses, SE Mediterranean Sea. *Global Planetary Change* 151, 60–67. doi: 10.1016/j.gloplacha.2016.04.001
- Ozsoy, E., Hecht, A., Ünlüata, Ü., Brenner, S., Sur, H. I., Bishop, J., et al. (1993). A synthesis of the levantine basin circulation and hydrograph—1990. *Deep-Sea Res.* 40, 1075–1119.
- Ozsoy, E., Unluata, U., Oguz, T., Latif, M. A., Hecht, A., Brenner, S., et al. (1991). A review of the levantine basin circulation and its variabilities during 1985–1988. *Dyn. Atmos. Oceans* 15, 421–456. doi: 10.1016/0377-0265(91)90027-D
- Pinardi, N., Cessi, P., Borile, F., and Wolfe, C. L. P. (2019). The Mediterranean Sea overturning circulation. *J. Phys. Oceanogr.* 49, 1699–1721. doi: 10.1175/JPO-D-18-0254.1
- Placenti, F., Torri, M., Pessini, F., Patti, B., Tancredi, V., Cuttitta, A., et al. (2022). Hydrological and biogeochemical patterns in the Sicily channel: New insights from the last decadal (2020). *Front. Mar. Sci.* 9. doi: 10.3389/fmars.2022.733540
- POEM Group (1992). General circulation of the Eastern Mediterranean. *Earth-Science Rev.* 32, 285–309. doi: 10.1016/0012-8252(92)90002-B
- Pollak, M. J. (1958). Frequency distribution of potential temperature and salinities in the Indian ocean. *Deep-Sea Res.* 5, 128–133. doi: 10.1016/0146-6313(58)90003-0
- Powley, H. R., Krom, M. D., Emeis, K.-C., and Van Cappellen, P. (2014). A biogeochemical model for phosphorus and nitrogen cycling in the Eastern Mediterranean Sea (EMS) part 2. response of nutrient cycles and primary production to anthropogenic forcing: 1950–2000. *J. Mar. Syst.* 139, 420–432. doi: 10.1016/j.jmarsys.2014.08.017
- Robinson, A. R., and Golnaraghi, M. (1993). Circulation and dynamics of the Eastern Mediterranean sea; quasi-synoptic data-driven simulations. *Deep Sea Res.* 40 (6), 1207–1246. doi: 10.1016/0967-0645(93)90068-X
- Robinson, A. R., Golnaraghi, M., Leslie, N., Artegiani, A., Hecht, A., Lazzone, E., et al. (1991). Structure and variability of the Eastern Mediterranean general circulation. *Dyn. Atmos. Oceans* 15, 215–240. doi: 10.1016/0377-0265(91)90021-7
- Robinson, A. R., Leslie, W. G., Theocharis, A., and Lascazatos, A. (2001). "Mediterranean Sea Circulation," in *Encyclopedia of ocean sciences* (Academic Press), 1689–1706. doi: 10.1006/rwos.2001.0376
- Rubino, A., Gacic, M., Bensi, M., Kovacevic, V., Malacic, V., Menna, M., et al. (2020). Experimental evidence of long-term oceanic circulation reversals without wind influence in the north Ionian Sea. *Sci. Rep.* 10, 1905. doi: 10.1038/s41598-020-57862-6
- Schlitzer, R., Roether, W., Oster, H., Junghans, H.-G., Hausmann, M., Johannsen, H., et al. (1991). Chlorofluoromethane and oxygen in the Eastern Mediterranean. *Deep-Sea Res.* 38.12, 1531–1551. doi: 10.1016/0198-0149(91)90088-W

- Schneider, A., Tanhua, T., Roether, W., and Steinfeldt, R. (2014). Changes in ventilation of the Mediterranean Sea during the past 25 year. *Ocean Sci.* 10, 1–16. doi: 10.5194/os-10-1-2014
- Schroeder, K., Garcia-Lafuente, J., Josey, S. A., Artale, V., Nardelli, B. B., Carrillo, A., et al. (2012). "Circulation of the Mediterranean Sea and its variability," in *The Mediterranean Climate : From past to future* (Amsterdam: Elsevier).
- Simon, M., Alldredge, A., and Azam, F. (1989). Protein-content and protein-synthesis rates of planktonic marine-bacteria. *Mar. Ecol. Prog. Ser.* 51, 201–213. doi: 10.3354/meps051201
- Sisma-Ventura, G., Bialik, O. M., Makovsky, Y., Rahav, E., Ozer, T., Kanari, M., et al. (2022). Cold seeps alter the near-bottom biogeochemistry in the ultraoligotrophic southeastern Mediterranean Sea. *Deep Sea Res. Part I: Oceanographic Res. Papers* 183, 103744. doi: 10.1016/j.dsr.2022.103744
- Smith, D. C., Smith, D. C., Azam, F., and Azam, F. (1992). A simple, economical method for measuring bacterial protein synthesis rates in seawater using 3H-leucine. *Mar. Microbial Food Webs* 6, 107–114.
- Steemann Nielsen, E. (1952). The use of radio-active carbon C14 for measuring organic production in the sea. *J. Con. Perm. Int. Explor. Mer* 18 (2), 117–140. doi: 10.1093/icesjms/18.2.117
- Tanhua, T., Hainbucher, D., Schroeder, K., Cardin, V., Alvarez, M., and Civitarese, G. (2013). The Mediterranean Sea system: a review and an introduction to the special issue. *Ocean Sci.* 9, 789–803. doi: 10.5194/os-9-789-2013
- Velaoras, D., Gogou, A., Zervoudaki, S., Civitarese, G., Giani, M., and Rahav, E. (2019). Revisiting the Eastern Mediterranean: Recent knowledge on the physical, biogeochemical and ecosystemic states and trends (Volume I). *Deep Sea Res. Part II* 164, 1–4. OI. doi: 10.1016/j.dsr2.2019.06.010
- Velaoras, V., Krokos, G., Nittis, K., and Theocharis, A. (2014). Dense intermediate water outflow from the Cretan Sea: A salinity driven, recurrent phenomenon, connected to thermohaline circulation changes. *J. Geophys. Res. Oceans* 119, 4797–4820. doi: 10.1002/2014JC009937
- Von Schuckmann, K., Le Traon, P.-Y., Smith, N., Pascual, A., Djavidnia, S., Gattuso, J.-P., et al. (2020). Copernicus Marine service ocean state report, issue 4. *J. Operational Oceanography* 13:sup1, s1–s172. doi: 10.1080/1755876X.2020.11785097
- Welschmeyer, N. A. (1994). Fluorometric analysis of chlorophyll a in the presence of chlorophyll b and pheopigments. *Limnology Oceanography* 39, 1985–1992. doi: 10.4319/lo.1994.39.8.1985
- Wust, G. (1961). On the vertical circulation of the Mediterranean Sea. *J. Geophys. Res.* 66, 3261–3271. doi: 10.1029/JZ066i010p03261